The ChiS family DNA-binding domain contains a cryptic helix-turn-helix variant

Catherine A. Klancher[1], George Minasov[2,3], Ram Podicheti[4], Douglas B. Rusch[4], Triana N. Dalia[1], Karla J. F. Satchell[2,3], Matthew B. Neiditch[5], Ankur B. Dalia[1,*]

[1]Department of Biology, Indiana University, Bloomington, IN, USA
[2]Department of Microbiology-Immunology, Feinberg School of Medicine, Northwestern University, Chicago, IL, USA
[3]Center for Structural Genomics of Infectious Diseases, Feinberg School of Medicine, Northwestern University, Chicago, IL, USA
[4]Center for Genomics and Bioinformatics, Indiana University, Bloomington, IN, USA.
[5]Department of Microbiology, Biochemistry, and Molecular Genetics, New Jersey Medical School, Rutgers Biomedical Health Sciences, Newark, NJ, USA
*Author for correspondence: ankdalia@indiana.edu

Abstract

Sequence specific DNA-binding domains (DBDs) are conserved in all domains of life. These proteins carry out a variety of cellular functions, and there are a number of distinct structural domains already described that allow for sequence-specific DNA binding, including the ubiquitous helix-turn-helix (HTH) domain. In the facultative pathogen *Vibrio cholerae*, the chitin sensor ChiS is a transcriptional regulator that is critical for the survival of this organism in its marine reservoir. We have recently shown that ChiS contains a cryptic DBD in its C-terminus. This domain is not homologous to any known DBD, but it is a conserved domain present in other bacterial proteins. Here, we present the crystal structure of the ChiS DBD at a resolution of 1.28 Å. We find that the ChiS DBD contains an HTH domain that is structurally similar to those found in other DNA binding proteins, like the LacI repressor. However, one striking difference observed in the ChiS DBD is that the canonical tight "turn" of the HTH is replaced with an extended loop containing a β-sheet, a variant which we term the "helix-sheet-helix". Through systematic mutagenesis of all positively charged residues within the ChiS DBD, we show that residues within and proximal to the ChiS helix-sheet-helix are critical for DNA binding. Finally, through phylogenetic analyses we show that the ChiS DBD is found in diverse Proteobacterial proteins that exhibit distinct domain architectures. Together, these results suggest that the structure described here represents the prototypical member of the ChiS-family of DBDs.

Importance

Regulating gene expression is essential in all domains of life. This process is commonly facilitated by the activity of DNA-binding transcription factors. There are diverse structural domains that allow proteins to bind to specific DNA sequences. The structural basis underlying how some proteins bind to DNA, however, remains unclear. Previously, we showed that in the major human pathogen *Vibrio cholerae*, the transcription factor ChiS directly regulates gene expression through a cryptic DNA binding domain. This domain lacked homology to any known DNA-binding protein. In the current study, we determined the structure of the ChiS DNA binding domain (DBD)

and find that the ChiS-family DBD is a cryptic variant of the ubiquitous helix-turn-helix (HTH) domain. We further demonstrate that this domain is conserved in diverse proteins that may represent a novel group of transcriptional regulators.

Introduction

The intestinal pathogen *Vibrio cholerae* natively resides in the aquatic environment and can cause disease if ingested in the form of contaminated food or drinking water. In the aquatic environment, *V. cholerae* commonly associates with the chitinous surfaces of crustacean zooplankton (1). Chitin is an abundant source of carbon and nitrogen for marine bacteria, including *V. cholerae* (2, 3). In addition, chitin serves as a cue to induce horizontal gene transfer by natural transformation in this species (4). Thus, *Vibrio*-chitin interactions are critical for this facultative pathogen to thrive and evolve in its environmental reservoir.

Chitin is sensed in *V. cholerae* by the hybrid histidine kinase ChiS (5-7). In response to chitin, ChiS activates the expression of the chitin utilization program. This regulon includes the *chb* operon, which is required for the uptake and degradation of the chitin disaccharide chitobiose. In a recent study, we showed that unlike most histidine kinases, ChiS is capable of directly binding to DNA to regulate the expression of the *chb* operon (5). This finding was particularly surprising because ChiS is not predicted to encode a DNA-binding domain *via* primary sequence homology (BLAST (8)) or structural predictions (Phyre2 (9)). In the current study, we sought to understand the structural basis for ChiS DNA binding. To that end, we determined the structure of the ChiS DBD and found that it encodes a distinct variant of the canonical helix-turn-helix domain, which we term a “helix-sheet-helix”.

Results and Discussion

The C-terminus of ChiS (ChiS$^{1024\text{-}1129}$) is sufficient to bind P_{chb}

Previous work from our group demonstrates that ChiS is a noncanonical hybrid histidine kinase that contains a DBD at its C-terminus (**Fig. 1A**) (5). In that study, we found that the C-terminal 106 amino acids of ChiS (ChiS$^{1024\text{-}1129}$) was necessary and sufficient to bind to the *chb* promoter *in vivo*. We further showed that ChiS binds directly to two binding sites within the *chb* operon promoter (P_{chb}) to activate the expression of this locus. To confirm that ChiS$^{1024\text{-}1129}$ was sufficient to bind DNA, we purified this domain and tested DNA-binding activity *in vitro* by electrophoretic mobility shift assays (EMSAs). We found that ChiS$^{1024\text{-}1129}$ bound to a wildtype P_{chb} promoter probe, but not to a probe in which the two ChiS binding sites were mutated, suggesting that this domain is sufficient to bind to DNA in a sequence-specific manner (**Fig. 1B** and **Fig. S1**). Thus, based on our *in vivo* and *in vitro* analysis, we refer to ChiS$^{1024\text{-}1129}$ as the ChiS DBD.

Identification of positively charged residues in the ChiS DBD that are critical for DNA binding and transcriptional activation of P_{chb}

As mentioned above, ChiS is not predicted to encode a DNA-binding domain based on *in silico* searches (*i.e.,* BLAST (8) and Phyre2 (9)). To characterize interactions between the ChiS DBD and DNA, we first tried to identify residues important for DNA binding.

The positively charged residues arginine (R) and lysine (K) commonly interact with the negatively charged DNA backbone (10). Thus, we mutated every R and K residue in the ChiS DBD to a glutamine (Q), to ablate their charge but maintain, to a reasonable extent, the steric properties of the side group.

To determine how these mutations affected ChiS activity, we introduced them into full-length FLAG-tagged ChiS (5), and assessed the ability of each mutant to bind to DNA *in vivo* (by chromatin immunoprecipitation, or ChIP) and to activate P_{chb} expression (using a P_{chb}-GFP reporter). We found that all mutations to the ChiS DBD reduced P_{chb}-GFP activation to varying degrees (**Fig. 2**). Most mutants were able to facilitate partial activation of P_{chb} and correspondingly partially enriched for P_{chb} by ChIP, indicating that they were binding to the promoter *in vivo*. Some mutants (R1068Q, R1074Q, K1078Q, R1090Q, and R1092Q) did not bind to P_{chb} DNA *in vivo* and resulted in complete loss of P_{chb} expression. Importantly, all mutants still produced ChiS protein as assessed by Western blot analysis (**Fig. S2**). Collectively, these data identify a subset of positively charged residues in the ChiS DBD that are critical for DNA binding and, subsequent transcriptional activation of the *chb* operon.

Structure of the ChiS DNA binding domain reveals a variant of the helix-turn-helix

We next sought to determine the structure of the ChiS DBD to further explore how ChiS interacts with DNA. Since no structures for close sequence homologs were available in the Protein Data Bank (PDB) to serve as search models for molecular replacement, we used the Single-wavelength Anomalous Dispersion (SAD) technique to determine initial phases. Selenomethionine was used as the replacement for methionine. Anomalous data were collected from a single crystal (**Tables S1 and S2**). The crystal diffracted to 1.28 Å resolution and belonged to the orthogonal $C222_1$ space group with unit cell parameters of a=51.91Å, b=78.61Å, c=72.37Å, $\alpha=\beta=\gamma=90.00°$. There was one polypeptide chain in the asymmetric unit. The structure includes 105 out of 106 residues of the protein (1024 – 1128), two uncleavable residues of the purification tag, four sulfate ions (SO_4^{2-}), one 2-(2-hydroxyethyloxy)ethanol molecule (PEG), two formic acids molecules (FMT) and 200 water molecules (HOH). Only the C-terminal E1129 was disordered in the structure and was not included in the final model.

The structure of the ChiS DBD revealed that it contains a fold that is reminiscent of the canonical helix-turn-helix (HTH) used by diverse DNA-binding proteins (**Fig. 3A-B**). The basic HTH domain consists of a trihelical bundle where the second and third helices encompass the namesake “helix-turn-helix” (11). The two helices that compose the HTH are connected *via* a relatively short linker that forms a sharp turn, which is a characteristic feature of this domain. Helix 3 from the HTH is generally inserted into the major groove of DNA, thus forming the principle DNA-protein interface. Alignment of the trihelical bundle from ChiS with the DNA-bound structure of the LacI repressor (PDB: 1EFA (12); RMSD of modeled C_α carbons = 3.514) revealed a similar spatial arrangement for each helix (**Fig. 3C**). Notably, however, the ChiS HTH has an extended loop between helix 2 and helix 3 that forms a beta sheet (**Fig. 3B-D**). Structural insertion between these helices is not typical; thus, the sheet found here is a distinct variant of the HTH which we refer to as a “helix-sheet-helix”.

Alignment of the ChiS DBD to LacI also revealed that the sheet within the ChiS helix-sheet-helix domain runs along the major groove (**Fig. 3C, 4A**), though it sterically conflicts with the DNA bases. This may suggest that the ChiS DBD takes on a slightly different conformation when bound to DNA. Consistent with this idea, the beta sheet has the highest B-factor (a measure of structural motion) in the ChiS DBD structure, indicating that it is relatively flexible (**Fig. 3E**). Thus, we speculate that this beta sheet is stabilized in the major groove when the ChiS DBD is bound to DNA. The unique helix-sheet-helix feature of the ChiS C-terminal domain may also explain why it was not previously identified as a DBD by structure prediction algorithms like Phyre2.

ChiS may bind to intrinsically bent DNA

Above, we identified five residues (R1068, R1074, K1078, R1090, and R1092) that were critical for the ChiS DBD to bind to DNA. Mapping these residues onto the ChiS DBD structure revealed that all five residues were found within the trihelical bundle that forms the helix-sheet-helix (**Fig. 4A**), which is consistent with this domain playing a critical role in DNA binding. Specifically, these residues were located in the beta sheet of the helix-sheet-helix (R1068), helix 3 (R1074, K1078), and helix 1 (R1090, R1092).

Most residues critical for DNA binding activity (R1068, R1074, K1078, R1090) were in close proximity to DNA on our modeled alignment; however, one residue (R1092), was distant from the DNA (**Fig. 4A**). Many transcription factors bend DNA upon binding to their target site (13, 14). Thus, one possible explanation for the critical role of R1092 is that the P_{chb} promoter is bent when bound by ChiS, which would allow for R1092 to come into close contact with DNA. To test this idea, we carried out a classic *in vitro* gel mobility shift assay to test DNA bending (15). This assay operates on the basis that the location of a bend within a DNA molecule alters its mobility during native PAGE analysis (16, 17). DNA probes that contain a bend in the middle of the probe exhibit the lowest mobility, while probes with the bend closer to one end show the highest mobility. Thus, we designed seven DNA probes of equal length that gradually shifted the position of the ChiS binding sites within the *chb* promoter (**Fig. 4B** and **Fig. S1**). First, we ran these probes in the absence of ChiS protein and found that they ran at different mobilities where the probes with the ChiS binding sites in the middle exhibited the lowest mobility (**Fig. 4C**). This suggested that the *chb* promoter likely has an intrinsic bend that is centered around the ChiS binding sites. The mobility pattern observed for these DNA probes did not change when incubated with the purified ChiS DBD (**Fig. S3**), suggesting that binding of the DNA probe by ChiS does not further bend the promoter. We propose that the *chb* promoter has an intrinsic bend, which may allow residues in the ChiS DBD, like R1092, to directly interact with DNA. The intrinsic bend found in the *chb* promoter may increase the affinity of ChiS for this region of DNA; indeed, DNA bending has been shown to increase the affinity of certain transcription factors for their DNA binding site (18).

The ChiS family DNA binding domain is associated with variable domain arrangements in diverse proteins

Above, we show that the ChiS DBD represents a cryptic variant of an HTH domain. As noted previously, the ChiS DBD is found in proteins other than homologs of ChiS (5). To more fully catalog proteins that contain this domain, we generated a profile Hidden Markov Model (HMM) to the ChiS DBD and screened for its presence among eubacterial genomes. A profile HMM is a position-specific scoring system that can effectively encode the variation in a training set of representative peptide sequences, and then find similar sequences from a much larger and more distantly related dataset compared to tools that do not require training, such as BLAST (19, 20).

This analysis revealed that the ChiS DBD is present in diverse Proteobacterial genomes (**Spreadsheet S1**). The vast majority of hits from our search were direct homologs of ChiS (3242/3829 = 84.7%), however, many proteins exhibited distinct domain architectures (587/3829 = 15.3%) (**Fig. 5A**). Strikingly, the ChiS DBD was found exclusively at the C-terminus in all of these proteins and was commonly associated with sensory domains (**Fig. 5A**). Furthermore, the helix-sheet-helix is highly conserved across these diverse proteins (**Fig. 5B, Spreadsheet S1**), and even the most dissimilar ChiS DBD homolog (MAC43155.1, bit score of 43.5; 22.6% identical, 43.4% similar to the ChiS DBD) still threaded (9) remarkably well onto the trihelical bundle of the ChiS DBD structure (RMSD of modeled C_α carbons = 0.002) (**Fig. S4**). Thus, it is tempting to speculate that ChiS is the founding member for a new group of DNA-binding transcription factors whose activity are regulated by diverse sensory inputs.

Materials & Methods

Bacterial strains and culture conditions

All *V. cholerae* strains used in this study are derived from the El Tor strain E7946 (21). *V. cholerae* strains were grown in LB medium and on LB agar supplemented when necessary with carbenicillin (20 μg/mL), kanamycin (50 μg/mL), spectinomycin (200 μg/mL), and/or trimethoprim (10 μg/mL). See **Table S3** for a detailed list of mutant strains used in this study.

Generating mutant strains

V. cholerae mutant constructs were generated using splicing-by-overlap extension exactly as previously described (22). See **Table S4** for all of the primers used to generate mutant constructs in this study. Mutant *V. cholerae* strains were generated by chitin-dependent natural transformation and cotransformation exactly as previously described (23). Mutant strains were confirmed by PCR and/or sequencing.

Cloning, protein production and purification

The *chiS*$^{1024\text{-}1129}$ (VC0622) construct was cloned into an Amp^R pET15b-based vector using the FastCloning method (24). This vector appended a TEV cleavable 6x His tag onto the N-terminus of ChiS$^{1024\text{-}1129}$. Vector and inserts were amplified using the primers listed in **Table S4**. The plasmid was transformed into *E. coli* BL21(DE3) (Magic) cells (25) and the protein was expressed in M9 media (High Yield M9 Se-Met media, Medicilon Inc.). The starting overnight culture was grown in LB medium supplemented with 130 μg/mL ampicillin and 50 μg/mL kanamycin at 37°C and 220 rpm. The next day,

M9 medium supplemented with 200 µg/mL ampicillin and 50 µg/mL kanamycin was inoculated with the overnight culture (1:100 dilution) and incubated at 37°C and 220 rpm. Protein expression was induced at OD_{600}=1.8-2.0 by the addition of 0.5 mM isopropyl β-d-1-thiogalactopyranoside and the culture was further incubated at 25°C, 200 rpm for 14 hours (26). The cells were harvested by centrifugation at 6,000 xg for 10 minutes, resuspended to 0.2 g/mL in lysis buffer (50 mM Tris pH 8.3, 0.5 M NaCl, 10% glycerol, 0.1% IGEPAL CA-630) and frozen at -30°C until purification.

Frozen pellets were thawed and sonicated at 50% amplitude, in a 5s on, 10s off cycle for 20 min at 4°C. The lysate was clarified by centrifugation at 18,000 xg for 40 minutes at 4°C and the supernatant was collected. The protein was purified in one step by IMAC followed by size exclusion chromatography using ÅKTAxpress system (GE Healthcare) as previously described with some modifications (27). The cell extract was loaded into a His-Trap FF (Ni-NTA) column with loading buffer (10 mM Tris-HCl pH 8.3, 500 mM NaCl, 1 mM Tris (2-carboxyethyl) phosphine (TCEP), 5% glycerol) and the column was washed with 10 column volumes of loading buffer and 10 column volumes of washing buffer (10 mM Tris-HCl pH 8.3, 1 M NaCl, 25 mM imidazole, 5% glycerol). Protein was eluted with elution buffer (10 mM Tris pH 8.3, 500 mM NaCl, 1 M imidazole), loaded onto a Superdex 200 26/600 column, separated in loading buffer, collected, and analyzed by PAGE. The 6x His tag was cleaved with recombinant TEV protease in a ratio of 1:20 (protein:protease) overnight at room temperature. The cleaved protein was separated from uncleaved protein, recombinant TEV protease, and 6x His tag peptide by Ni-NTA-affinity chromatography using loading buffer followed by loading buffer with 25 mM imidazole. The cleaved protein was collected in the flow-through in both the loading buffer and the loading buffer with 25 mM imidazole. Both fractions were analyzed by PAGE for 6x His tag cleavage, concentrated to 6-8 mg/mL, and set up for crystallization.

Crystallization, data collection, structure solution and refinement

The protein from both fractions (collected in flow through and in 25 mM imidazole) was set up at 6-8 mg/mL in loading buffer containing 0 or 500 mM NaCl as 2 µL crystallization drops (1 µL protein: 1 µL reservoir solution) in 96-well plates (Corning) using commercial Classics II, PACT and JCSG+ (QIAGEN) crystallization screens. Diffraction quality crystal of the protein collected with 25 mM imidazole grown from the condition with 0.2 M lithium sulfate, 0.1 M Bis-Tris, pH 5.5, 25%(w/v) PEG 3350 (Classics II, #74) was flash frozen in liquid nitrogen for data collection.

The crystals were screened, and data were collected at the Life Sciences-Collaborative Access Team (LS-CAT) beamline F at the Advanced Photon Source (APS) of the Argonne National Laboratory. A total of 300 diffraction images were indexed, integrated and scaled using HKL-3000 (28). The structure was determined with the HKL3000 structure solution package using anomalous signal from selenomethionine (Se-Met). The initial model went through several rounds of refinement in REFMAC v. 5.8.0258 (29) and manual corrections in Coot (30). The water molecules were generated using ARP/wARP (31) and ligands were added to the model manually during visual inspection in Coot. Translation–Libration–Screw (TLS) groups were created by the TLSMD server

(32) and TLS corrections were applied during the final stages of refinement. MolProbity (33) was used for monitoring the quality of the model during refinement and for the final validation of the structure. The structure was deposited to the Protein Data Bank (https://www.rcsb.org/) with the assigned PDB code 7KPO.

Electrophoretic mobility shift assay (EMSA)

Binding reactions contained 10 mM Tris HCl pH 7.5, 1 mM EDTA, 10 mM KCl, 1 mM DTT, 50 µg/mL BSA, 0.1 mg/mL salmon sperm DNA, 5% glycerol, 1 nM of a Cy5 labeled DNA probe, and purified ChiS DBD at the indicated concentrations (diluted in 10 mM Tris pH 7.5, 10 mM KCl, 1 mM DTT, and 5% glycerol). Reactions were incubated at room temperature for 20 minutes in the dark, then electrophoretically separated on polyacrylamide gels in 0.5x Tris Borate EDTA (TBE) buffer at 4°C. Gels were imaged for Cy5 fluorescence on a Typhoon-9210 instrument. Cy5-labeled P_{chb} probes were made by Phusion PCR, where Cy5-dCTP was included in the reaction at a level that would result in incorporation of 1–2 Cy5 labeled nucleotides in the final probe as previously described (22).

Measuring GFP reporter fluorescence

GFP fluorescence was determined essentially as previously described (34). Briefly, single colonies were picked and grown in LB broth at 30°C for 18 hours. Cells were then washed and resuspended to an OD_{600} of 1.0 in instant ocean medium (7 g/L; Aquarium Systems). Then, fluorescence was determined using a BioTek H1M plate reader with excitation set to 500 nm and emission set to 540 nm.

Chromatin immunoprecipitation (ChIP)-qPCR assays

ChIP assays were carried out exactly as previously described (5). Briefly, overnight cultures were diluted to an OD_{600} of 0.08 and then grown for 6 hours at 30°C. Cultures were crosslinked using 1% paraformaldehyde, then quenched with a 1.2 molar excess of Tris. Cells were washed with PBS and stored at -80°C overnight. The next day, cells were resuspended in lysis buffer (1x FastBreak cell lysis reagent (Promega), 50 µg/mL lysozyme, 1% Triton X-100, 1 mM PMSF, and 1x protease inhibitor cocktail; 100x inhibitor cocktail contained the following: 0.07 mg/mL phosphoramidon (Santa Cruz), 0.006 mg/mL bestatin (MPbiomedicals/Fisher Scientific), 1.67 mg/mL AEBSF (DOT Scientific), 0.07 mg/mL pepstatin A (Gold Bio), 0.07 mg/mL E64 (Gold Bio)) and then lysed by sonication, resulting in a DNA shear size of ~500 bp. Lysates were incubated with Anti-FLAG M2 Magnetic Beads (Sigma), washed to remove unbound proteins, and then bound protein-DNA complexes were eluted off with SDS. Samples were digested with Proteinase K, then crosslinks were reversed. DNA samples were cleaned up and used as template for quantitative PCR (qPCR) using iTaq Universal SYBR Green Supermix (Bio-Rad) and primers specific for the genes indicated (see **Table S4** for primers) on a Step-One qPCR system. Standard curves of genomic DNA were included in each experiment and were used to determine the abundance of each amplicon in the input (derived from the lysate prior to ChIP) and output (derived from the samples after ChIP). Primers to amplify *rpoB* served as a baseline control in this assay because ChiS does not bind this locus. Data are reported as 'Fold Enrichment', which is defined as the ratio of P_{chb} / *rpoB* found in the output divided by the same ratio found in the input.

Western blot analysis

Strains were grown as described for ChIP assays, pelleted, resuspended, and boiled in 1x SDS PAGE sample buffer (110 mM Tris pH 6.8, 12.5% glycerol, 0.6% SDS, 0.01% Bromophenol Blue, and 2.5% β-mercaptoethanol). Proteins were separated by SDS polyacrylamide gel electrophoresis, then transferred to a PVDF membrane, and probed with rabbit polyconal α-FLAG (Sigma) or mouse monoclonal α-RpoA (Biolegend) primary antibodies. Blots were then incubated with α-rabbit or α-mouse HRP conjugated secondary antibodies, developed using Pierce ECL 529 Western Blotting Substrate (ThermoFisher), and imaged on a ProteinSimple Fluorchem E instrument.

Bioinformatic identification of eubacterial proteins with putative ChiS DBD domains

The DBD sequence segments from the protein sequences of seven ChiS DNA binding domain homologs (THB81618.1, OGG93021.1, OUR95018.1, WP_084205767.1, ODU31202.1, WP_070993003.1, WP_078715702.1) (5) were aligned using MUSCLE version 3.8.31 (35). The resulting multiple sequence alignment was turned into a profile HMM which was searched against the eubacterial subset (taxonomy id: 2) of NCBI non-redundant protein sequence database using HMMER version 3.2.1 (http://hmmer.org/), requiring the alignment length to be at least 90. Among the hits, proteins sequences tagged “partial” in their FASTA headers were excluded. Domain architectures for the remaining hits were obtained from the NLM conserved domain database (36). Any protein hits with regions aligned to the DNA binding domain HMM overlapping with known annotated functional domains were excluded. The resulting ChiS DBD homolog protein sequences were clustered using cd-hit ver. v4.8.1-2019-0228 (37) (parameters: -M 0 -g 1 -s 0.8 -c 0.4 -n 2 -d 500). Clusters identified by cd-hit were further grouped together by manually analyzing the domain architecture of hits as shown in **Fig. 5A**. Only clusters containing 10 or more representatives were grouped, while the remaining proteins were left unassigned. For a list of all proteins containing a putative ChiS DBD, see **Spreadsheet S1**.

Acknowledgements

We thank Dipankar Sen, Julia van Kessel, and Ryan Chaparian for helpful discussions. We thank Olga Kiryukhina, Grant Wiersum, Ivgeniia Dubrovska, and Ludmilla Shuvalova for assistance on protein crystallization. This work was supported by grant R35GM128674 from the National Institutes of Health (to ABD) and, in part, with Federal funds from the Department of Health and Human Services. National Institutes of Health, National Institute of Allergy and Infectious Diseases under Contract No. HHSN272201700060C (to KJFS). This research used resources of the Advanced Photon Source, a U.S. Department of Energy (DOE) Office of Science User Facility operated for the DOE Office of Science by Argonne National Laboratory under Contract No. DE-AC02-06CH11357. Use of the LS-CAT Sector 21 was supported by the Michigan Economic Development Corporation and the Michigan Technology Tri-Corridor (Grant 085P1000817). This research was supported in part by Lilly Endowment, Inc., through its support for the Indiana University Pervasive Technology Institute.

References

1. Pruzzo C, Vezzulli L, Colwell RR. Global impact of Vibrio cholerae interactions with chitin. Environ Microbiol. 2008;10(6):1400-10.
2. Hunt DE, Gevers D, Vahora NM, Polz MF. Conservation of the chitin utilization pathway in the Vibrionaceae. Appl Environ Microbiol. 2008;74(1):44-51.
3. Nahar S, Sultana M, Naser MN, Nair GB, Watanabe H, Ohnishi M, et al. Role of Shrimp Chitin in the Ecology of Toxigenic Vibrio cholerae and Cholera Transmission. Front Microbiol. 2011;2:260.
4. Meibom KL, Blokesch M, Dolganov NA, Wu CY, Schoolnik GK. Chitin induces natural competence in Vibrio cholerae. Science. 2005;310(5755):1824-7.
5. Klancher CA, Yamamoto S, Dalia TN, Dalia AB. ChiS is a noncanonical DNA-binding hybrid sensor kinase that directly regulates the chitin utilization program in Vibrio cholerae. Proc Natl Acad Sci U S A. 2020;117(33):20180-9.
6. Li X, Roseman S. The chitinolytic cascade in Vibrios is regulated by chitin oligosaccharides and a two-component chitin catabolic sensor/kinase. Proc Natl Acad Sci U S A. 2004;101(2):627-31.
7. Meibom KL, Li XB, Nielsen AT, Wu CY, Roseman S, Schoolnik GK. The Vibrio cholerae chitin utilization program. Proc Natl Acad Sci U S A. 2004;101(8):2524-9.
8. Altschul SF, Gish W, Miller W, Myers EW, Lipman DJ. Basic local alignment search tool. J Mol Biol. 1990;215(3):403-10.
9. Kelley LA, Mezulis S, Yates CM, Wass MN, Sternberg MJ. The Phyre2 web portal for protein modeling, prediction and analysis. Nat Protoc. 2015;10(6):845-58.
10. Luscombe NM, Laskowski RA, Thornton JM. Amino acid-base interactions: a three-dimensional analysis of protein-DNA interactions at an atomic level. Nucleic Acids Res. 2001;29(13):2860-74.
11. Aravind L, Anantharaman V, Balaji S, Babu MM, Iyer LM. The many faces of the helix-turn-helix domain: transcription regulation and beyond. FEMS Microbiol Rev. 2005;29(2):231-62.
12. Bell CE, Lewis M. A closer view of the conformation of the Lac repressor bound to operator. Nat Struct Biol. 2000;7(3):209-14.
13. Vamosi G, Rueda D. DNA Bends the Knee to Transcription Factors. Biophys J. 2018;114(10):2253-4.
14. van der Vliet PC, Verrijzer CP. Bending of DNA by transcription factors. Bioessays. 1993;15(1):25-32.
15. Kim J, Zwieb C, Wu C, Adhya S. Bending of DNA by gene-regulatory proteins: construction and use of a DNA bending vector. Gene. 1989;85(1):15-23.
16. Koo HS, Wu HM, Crothers DM. DNA bending at adenine . thymine tracts. Nature. 1986;320(6062):501-6.
17. Wu HM, Crothers DM. The locus of sequence-directed and protein-induced DNA bending. Nature. 1984;308(5959):509-13.
18. Afek A, Shi H, Rangadurai A, Sahay H, Senitzki A, Xhani S, et al. DNA mismatches reveal conformational penalties in protein-DNA recognition. Nature. 2020.
19. Yoon BJ. Hidden Markov Models and their Applications in Biological Sequence Analysis. Curr Genomics. 2009;10(6):402-15.

20. Altschul SF, Madden TL, Schaffer AA, Zhang J, Zhang Z, Miller W, et al. Gapped BLAST and PSI-BLAST: a new generation of protein database search programs. Nucleic Acids Res. 1997;25(17):3389-402.
21. Miller VL, DiRita VJ, Mekalanos JJ. Identification of toxS, a regulatory gene whose product enhances toxR-mediated activation of the cholera toxin promoter. J Bacteriol. 1989;171(3):1288-93.
22. Dalia AB, Lazinski DW, Camilli A. Characterization of undermethylated sites in Vibrio cholerae. J Bacteriol. 2013;195(10):2389-99.
23. Dalia AB. Natural Cotransformation and Multiplex Genome Editing by Natural Transformation (MuGENT) of Vibrio cholerae. Methods Mol Biol. 2018;1839:53-64.
24. Li C, Wen A, Shen B, Lu J, Huang Y, Chang Y. FastCloning: a highly simplified, purification-free, sequence- and ligation-independent PCR cloning method. BMC Biotechnol. 2011;11:92.
25. Kwon K, Peterson SN. High-throughput cloning for biophysical applications. Methods Mol Biol. 2014;1140:61-74.
26. Millard CS, Stols L, Quartey P, Kim Y, Dementieva I, Donnelly MI. A less laborious approach to the high-throughput production of recombinant proteins in Escherichia coli using 2-liter plastic bottles. Protein Expr Purif. 2003;29(2):311-20.
27. Shuvalova L. Parallel protein purification. Methods Mol Biol. 2014;1140:137-43.
28. Minor W, Cymborowski M, Otwinowski Z, Chruszcz M. HKL-3000: the integration of data reduction and structure solution--from diffraction images to an initial model in minutes. Acta Crystallogr D Biol Crystallogr. 2006;62(Pt 8):859-66.
29. Murshudov GN, Skubak P, Lebedev AA, Pannu NS, Steiner RA, Nicholls RA, et al. REFMAC5 for the refinement of macromolecular crystal structures. Acta Crystallogr D Biol Crystallogr. 2011;67(Pt 4):355-67.
30. Emsley P, Cowtan K. Coot: model-building tools for molecular graphics. Acta Crystallogr D Biol Crystallogr. 2004;60(Pt 12 Pt 1):2126-32.
31. Morris RJ, Perrakis A, Lamzin VS. ARP/wARP and automatic interpretation of protein electron density maps. Methods Enzymol. 2003;374:229-44.
32. Painter J, Merritt EA. Optimal description of a protein structure in terms of multiple groups undergoing TLS motion. Acta Crystallogr D Biol Crystallogr. 2006;62(Pt 4):439-50.
33. Chen VB, Arendall WB, 3rd, Headd JJ, Keedy DA, Immormino RM, Kapral GJ, et al. MolProbity: all-atom structure validation for macromolecular crystallography. Acta Crystallogr D Biol Crystallogr. 2010;66(Pt 1):12-21.
34. Dalia AB. RpoS is required for natural transformation of Vibrio cholerae through regulation of chitinases. Environ Microbiol. 2016;18(11):3758-67.
35. Edgar RC. MUSCLE: a multiple sequence alignment method with reduced time and space complexity. BMC Bioinformatics. 2004;5:113.
36. Lu S, Wang J, Chitsaz F, Derbyshire MK, Geer RC, Gonzales NR, et al. CDD/SPARCLE: the conserved domain database in 2020. Nucleic Acids Res. 2020;48(D1):D265-D8.
37. Li W, Godzik A. Cd-hit: a fast program for clustering and comparing large sets of protein or nucleotide sequences. Bioinformatics. 2006;22(13):1658-9.

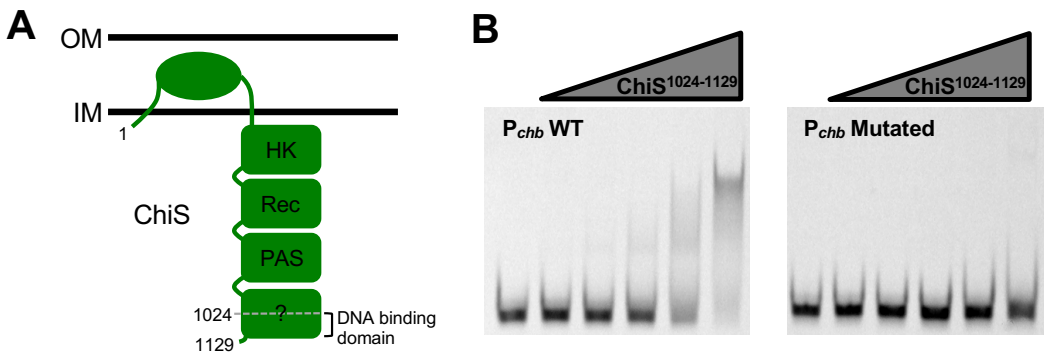

Figure 1. *The C-terminus of ChiS (ChiS$^{1024-1129}$) is sufficient to bind P_{chb}*. **A**) Diagram of the domain architecture for the hybrid histidine kinase ChiS. ChiS contains a histidine kinase (HK) domain, a receiver domain (Rec), a PAS domain, and a domain that does not have homology to known domains. Residues 1024-1129 were previously shown to be sufficient to bind P_{chb} *in vivo* (5). **B**) A fragment of the ChiS C-terminus (ChiS$^{1024-1129}$) was purified and assessed for DNA binding activity by EMSA. Purified protein was incubated with the indicated Cy5-labeled 60 bp probes containing sequence from P_{chb} encompassing the two ChiS binding sites (CBSs). A promoter map with the region of the promoter used for EMSAs are diagrammed in **Figure S1A**. The concentration of ChiS used (from left to right) was 0 nM, 25 nM , 50 nM, 100 nM, 200 nM, and 400 nM. The probe sequence was WT (P_{chb} WT) or the CBSs were both mutated (P_{chb} Mutated). Data are representative of two independent experiments.

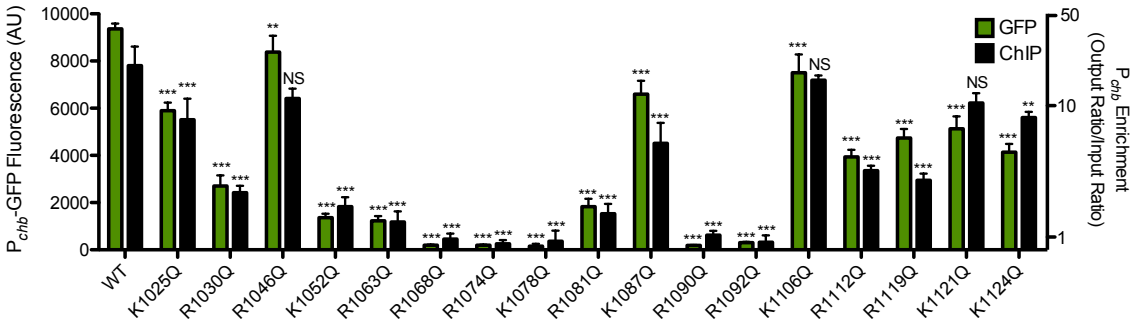

Figure 2. *Identification of positively charged residues in the ChiS DBD that are critical for DNA binding and transcriptional activation of P_{chb}.* All lysines and arginines in the ChiS DNA binding domain were individually mutated to a glutamine and ChiS was assessed for (1) transcriptional activation of a P_{chb}-GFP reporter (green bars; left Y-axis) and (2) ChiS binding to P_{chb} *in vivo* by chromatin immunoprecipitation (ChIP) (black bars; right Y-axis). ChiS can be activated with its native inducer, chitin, or by deletion of its periplasmic regulator, CBP; here, ChiS was activated artificially by deleting CBP. Data are the result of at least three independent biological replicates and are shown as the mean ± SD. Statistical markers indicated directly above bars indicate comparisons to the WT. Statistical comparisons were made by one-way ANOVA with Tukey's Posttest. ***, $p < 0.001$; ** $p < 0.01$; NS, not significant.

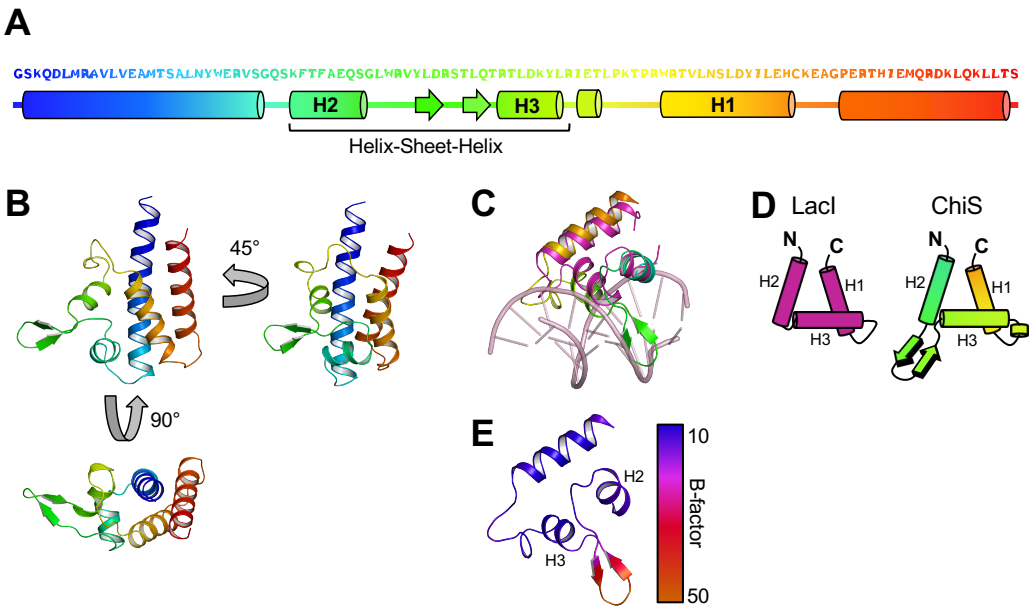

Figure 3. *Structure of the ChiS DNA binding domain reveals a variant of the helix-turn-helix.* **A**) Domain architecture of the ChiS DNA binding domain. The primary sequence of the ChiS DBD (S1024-S1128) is shown. Helices are depicted as cylinders, while sheets are depicted as arrows. **B**) Crystal structure of the ChiS DNA binding domain. The structural elements are colored coded as depicted in the primary sequence in **B**. **C**) Alignment of the ChiS trihelical bundle (rainbow) with the LacI triehlical bundle bound to the LacI operator site (PDB: 1EFA; pink). Alignment of alpha carbons gave an RMSD of 3.514. **D**) Cartoon representations of the trihelical bundle from LacI and ChiS. Helices are labeled with nomenclature presented in Aravind, *et. al.* (11). **E**) Structure of the ChiS trihelical bundle colored to represent B-factor. Helices found in the helix-sheet-helix motif (H2 and H3) are indicated.

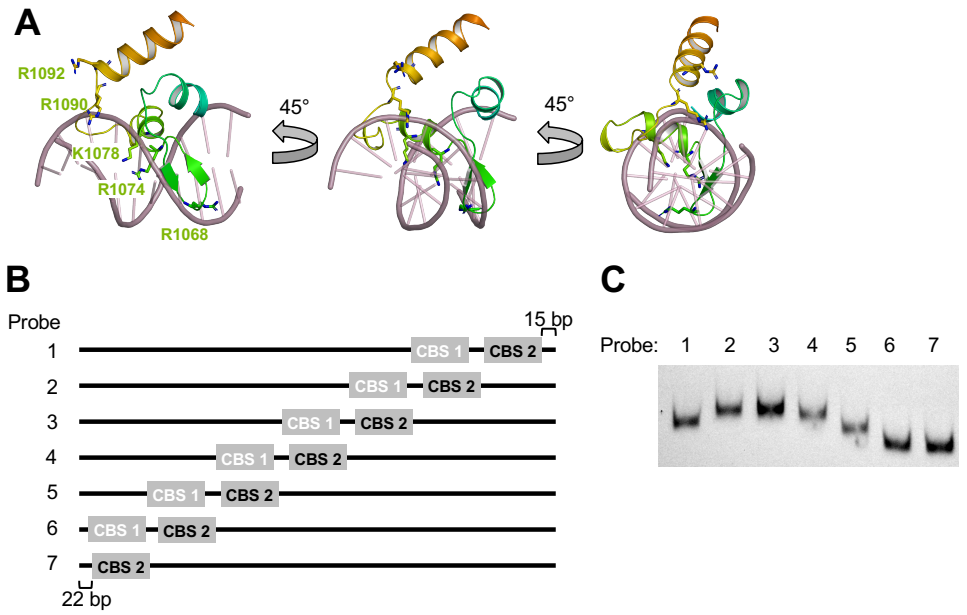

Figure 4. *ChiS may bind to intrinsically bent DNA.* **A**) Model of the ChiS trihelical bundle bound to double-stranded DNA from the alignment shown in **Figure 3C**. Side chains for the residues critical for DNA binding (R1068, R1074, K1078, R1090, and R1092) are shown and indicated. **B**) Diagram of the 7 distinct 230 bp probes used in **C**. ChiS binding site 1 (CBS 1) was mutated (white text) and ChiS binding site 2 (CBS 2) was left intact (black text). CBS 2 was shifted by 30 bp between each probe. **C**) The DNA probes diagrammed in **B** were labeled with Cy5 and separated by native PAGE in the absence of ChiS protein.

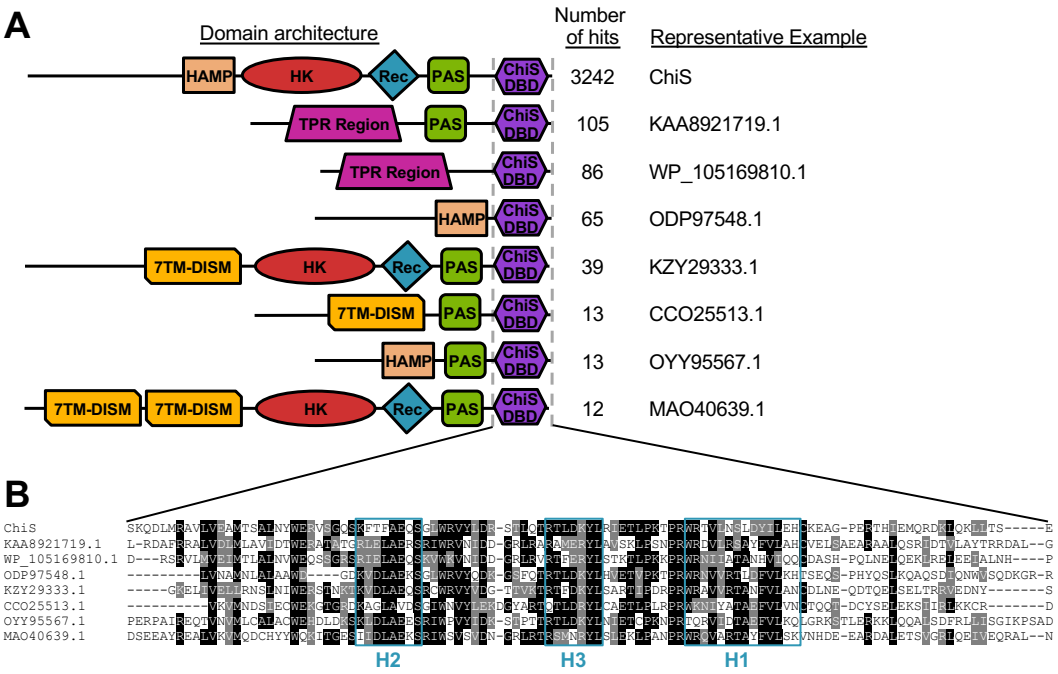

Figure 5. *The ChiS family DBD is found in diverse proteins with distinct domain architectures among Proteobacterial genomes.* **A**) Diagrams of the most abundant protein architectures containing the ChiS family DBD. Protein domains shown are HAMP, Histidine Kinase (HK), Receiver (Rec), Per-Arnt-Sim (PAS), Tetratricopeptide Repeat (TPR), 7 Transmembrane Receptors with Diverse Intracellular Signaling Modules (7TMR-DISM), and the ChiS family DNA binding domain (ChiS DBD). For a complete list of hits containing the indicated architectures see **Spreadsheet S1**. **B**) Alignment of the primary sequences of the ChiS family DBD in the indicated proteins are shown. Residues in black are identical, while those in gray are similar. The sequence for helix 1 (H1), helix 2 (H2) and helix 3 (H3) are boxed in teal.

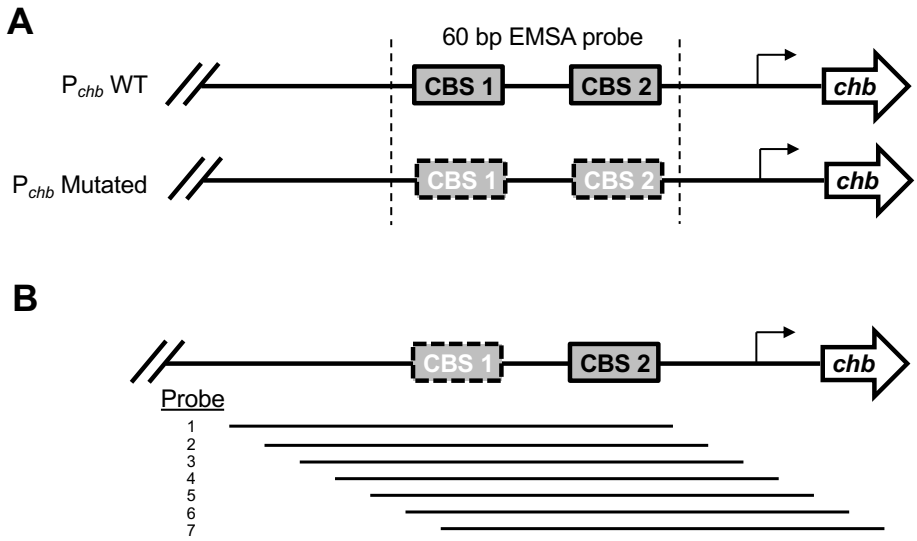

Figure S1. *Diagrams of EMSA probes used in this study.* **A**) Promoter map of *chb* with the region of P_{chb} used for the EMSAs shown in **Figure 1B** indicated. ChiS binding sites (CBSs) were left intact (black text, solid line) or mutated (white text, dotted line). **B**) Promoter map of *chb* with the region of P_{chb} used for the EMSA shown in **Figure 4C** and **Figure S3**. CBS 1 was mutated in all probes used.

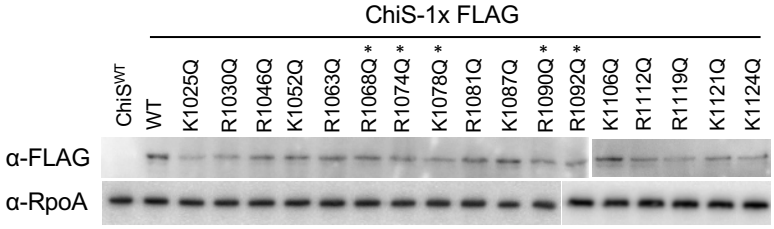

Figure S2. *Mutations to the ChiS DNA binding domain does not prevent expression of ChiS.* Strains expressing the indicated ChiS-FLAG point mutations were assessed for expression by Western blot with anti-FLAG and anti-RpoA (loading control) antibodies. Asterisks above ChiS point mutants indicate the mutations found to be critical for the DNA binding activity of ChiS in **Figure 2**.

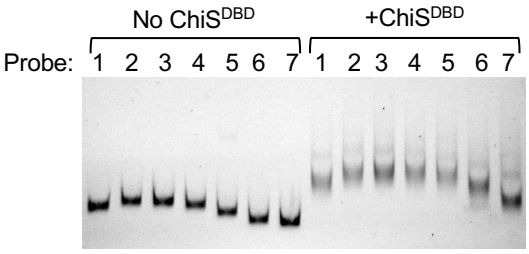

Figure S3. *ChiS protein does not further bend the P_{chb} promoter.* The probes shown in **Figure S1B** were incubated in the absence (No ChiS^{DBD}) or presence (+ChiS^{DBD}) of 400 nM ChiS^{DBD}.

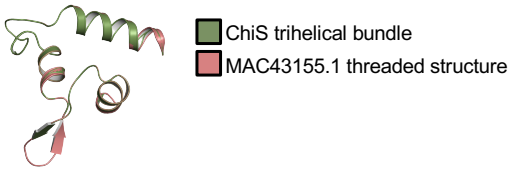

Figure S4. *The most dissimilar ChiS DBD homolog threads onto the trihelical bundle of the ChiS DBD structure.* The sequence of the ChiS-family DBD from MAC43155.1 was threaded onto the crystal structure of the ChiS DBD using Phyre2 (9). Alignment of alpha carbons gave an RMSD of 0.002.

Table S1. Data collection and processing

Values in parentheses are for the outer shell.

Diffraction source	Beamline 21ID-F, APS
Wavelength (Å)	0.97872
Temperature (K)	100
Detector	MAR Mosaic 300 mm CCD
Space group	$C222_1$
a, b, c (Å)	51.91, 78.61, 72.37
α, β, γ (°)	90.00, 90.00, 90.00
Resolution range (Å)	30.00 - 1.28 (1.30 - 1.28)
No. of unique reflections	38,590 (1,866)
Completeness (%)	99.7 (97.3)
Multiplicity	6.9 (4.6)
⟨I/σ(I)⟩	28.3 (2.3)
$R_{r.i.m.}$ †	0.032 (0.386)
$CC_{1/2}$††	(0.637)
Overall B factor from Wilson plot (Å^2)	14.7

†Estimated $R_{r.i.m.} = R_{merge}[N/(N-1)]^{1/2}$, where N is the data multiplicity.

†† Pearson's Correlation Coefficient (Karplus & Diederichs, 2012).

Table S2. Structure refinement

Values in parentheses are for the outer shell.

Resolution range (Å)	25.97 - 1.28 (1.31 - 1.28)
Completeness (%)	99.7 (98.3)
No. of reflections, working set	36,482 (2,634)
No. of reflections, test set	1,885 (138)
Final R_{work}	0.144 (0.214)
Final R_{free}	0.180 (0.238)
No. of non-H atoms	
Protein	989
Ligand	33
Water	200
Total	1,222
R.m.s. deviations	
Bonds (Å)	0.005
Angles (°)	1.217
Average B factors ($Å^2$)	
Protein	17.8
Ligand	31.6
Water	31.3
Ramachandran plot	
Favored regions (%)	99.0
Additionally allowed (%)	1.0
Outliers (%)	0.0

Table S3. *Strains used in this study.*

Strain (Reference)	Reference in Manuscript	Genotype
SAD 030	Parent strain for all other *V. cholerae* strains in this study	*V. cholerae* E7946 WT Sm^R
SAD 2706	Figure 2 ChIP WT & Figure S1 WT	Δ*lacZ*::P_{chb}-GFP, Kan^R; Δ*chiS/cbp*::$Carb^R$; ΔVCA0692::ChiS 1x FLAG @ E566, TmR
SAD 3006	Figure 2 ChIP K1025Q & Figure S1 K1025Q	Δ*lacZ*::P_{chb}-GFP, Kan^R; Δ*chiS/cbp*::$Carb^R$; ΔVCA0692::ChiS 1x FLAG @ E566 K1025Q, Tm^R
SAD 3007	Figure 2 ChIP R1030Q & Figure S1 R1030Q	Δ*lacZ*::P_{chb}-GFP, Kan^R; Δ*chiS/cbp*::$Carb^R$; ΔVCA0692::ChiS 1x FLAG @ E566 R1030Q, Tm^R
SAD 3008	Figure 2 ChIP R1046Q & Figure S1 R1046Q	Δ*lacZ*::P_{chb}-GFP, Kan^R; Δ*chiS/cbp*::$Carb^R$; ΔVCA0692::ChiS 1x FLAG @ E566 R1046Q, Tm^R
SAD 3009	Figure 2 ChIP K1052Q & Figure S1 K1052Q	Δ*lacZ*::P_{chb}-GFP, Kan^R; Δ*chiS/cbp*::$Carb^R$; ΔVCA0692::ChiS 1x FLAG @ E566 K1052Q, Tm^R
SAD 3010	Figure 2 ChIP R1063Q & Figure S1 R1063Q	Δ*lacZ*::P_{chb}-GFP, Kan^R; Δ*chiS/cbp*::$Carb^R$; ΔVCA0692::ChiS 1x FLAG @ E566 R1063Q, Tm^R
SAD 3011	Figure 2 ChIP R1068Q & Figure S1 R1068Q	Δ*lacZ*::P_{chb}-GFP, Kan^R; Δ*chiS/cbp*::$Carb^R$; ΔVCA0692::ChiS 1x FLAG @ E566 R1068Q, Tm^R
SAD 3012	Figure 2 ChIP R1074Q & Figure S1 R1074Q	Δ*lacZ*::P_{chb}-GFP, Kan^R; Δ*chiS/cbp*::$Carb^R$; ΔVCA0692::ChiS 1x FLAG @ E566 R1074Q, Tm^R
SAD 3013	Figure 2 ChIP K1078Q & Figure S1 K1078Q	Δ*lacZ*::P_{chb}-GFP, Kan^R; Δ*chiS/cbp*::$Carb^R$; ΔVCA0692::ChiS 1x FLAG @ E566 K1078Q, Tm^R
SAD 3014	Figure 2 ChIP R1081Q & Figure S1 R1081Q	Δ*lacZ*::P_{chb}-GFP, Kan^R; Δ*chiS/cbp*::$Carb^R$; ΔVCA0692::ChiS 1x FLAG @ E566 R1081Q, Tm^R
SAD 3015	Figure 2 ChIP K1087Q & Figure S1 K1087Q	Δ*lacZ*::P_{chb}-GFP, Kan^R; Δ*chiS/cbp*::$Carb^R$; ΔVCA0692::ChiS 1x FLAG @ E566 K1087Q, Tm^R
SAD 3016	Figure 2 ChIP R1090Q & Figure S1 R1090Q	Δ*lacZ*::P_{chb}-GFP, Kan^R; Δ*chiS/cbp*::$Carb^R$; ΔVCA0692::ChiS 1x FLAG @ E566 R1090Q, Tm^R
SAD 3017	Figure 2 ChIP R1092Q & Figure S1 R1092Q	Δ*lacZ*::P_{chb}-GFP, Kan^R; Δ*chiS/cbp*::$Carb^R$; ΔVCA0692::ChiS 1x FLAG @ E566 R1092Q, Tm^R
SAD 3018	Figure 2 ChIP K1106Q & Figure S1 K1106Q	Δ*lacZ*::P_{chb}-GFP, Kan^R; Δ*chiS/cbp*::$Carb^R$; ΔVCA0692::ChiS 1x FLAG @ E566 K1106Q, Tm^R
SAD 3019	Figure 2 ChIP R1112Q & Figure S1 R1112Q	Δ*lacZ*::P_{chb}-GFP, Kan^R; Δ*chiS/cbp*::$Carb^R$; ΔVCA0692::ChiS 1x FLAG @ E566 R1112Q, Tm^R
SAD 3020	Figure 2 ChIP R1119Q & Figure S1 R1119Q	Δ*lacZ*::P_{chb}-GFP, Kan^R; Δ*chiS/cbp*::$Carb^R$; ΔVCA0692::ChiS 1x FLAG @ E566 R1119Q, Tm^R
SAD 3021	Figure 2 ChIP K1121Q & Figure S1 K1121Q	Δ*lacZ*::P_{chb}-GFP, Kan^R; Δ*chiS/cbp*::$Carb^R$; ΔVCA0692::ChiS 1x FLAG @ E566 K1121Q, Tm^R
SAD 3022	Figure 2 ChIP K1124Q & Figure S1 K1124Q	Δ*lacZ*::P_{chb}-GFP, Kan^R; Δ*chiS/cbp*::$Carb^R$; ΔVCA0692::ChiS 1x FLAG @ E566 K1124Q, Tm^R
SAD 3023	Figure 2 GFP WT	Δ*lacZ*::P_{chb}-GFP, Kan^R; igVCA0265/0266::CBS-mCherry v2, Cm^R; ΔchiS/cbp::$Carb^R$; ΔVCA0692::ChiS, Tm^R
SAD 3024	Figure 2 GFP K1025Q	Δ*lacZ*::P_{chb}-GFP, Kan^R; igVCA0265/0266::CBS-mCherry v2, Cm^R; ΔchiS/cbp::$Carb^R$; ΔVCA0692::ChiS K1025Q, Tm^R
SAD 3025	Figure 2 GFP R1030Q	Δ*lacZ*::P_{chb}-GFP, Kan^R; igVCA0265/0266::CBS-mCherry v2, Cm^R; ΔchiS/cbp::$Carb^R$; ΔVCA0692::ChiS R1030Q, Tm^R
SAD 3026	Figure 2 GFP R1046Q	Δ*lacZ*::P_{chb}-GFP, Kan^R; igVCA0265/0266::CBS-mCherry v2, Cm^R; ΔchiS/cbp::$Carb^R$; ΔVCA0692::ChiS R1046Q, Tm^R

SAD 3027	Figure 2 GFP K1052Q	Δ*lacZ*::P_{chb}-GFP, Kan^R; igVCA0265/0266::CBS-mCherry v2, Cm^R; ΔchiS/cbp::$Carb^R$; ΔVCA0692::ChiS K1052Q, Tm^R
SAD 3028	Figure 2 GFP R1063Q	Δ*lacZ*::P_{chb}-GFP, Kan^R; igVCA0265/0266::CBS-mCherry v2, Cm^R; ΔchiS/cbp::$Carb^R$; ΔVCA0692::ChiS R1063Q, Tm^R
SAD 3029	Figure 2 GFP R1068Q	Δ*lacZ*::P_{chb}-GFP, Kan^R; igVCA0265/0266::CBS-mCherry v2, Cm^R; ΔchiS/cbp::$Carb^R$; ΔVCA0692::ChiS R1068Q, Tm^R
SAD 3030	Figure 2 GFP R1074Q	Δ*lacZ*::P_{chb}-GFP, Kan^R; igVCA0265/0266::CBS-mCherry v2, Cm^R; ΔchiS/cbp::$Carb^R$; ΔVCA0692::ChiS R1074Q, Tm^R
SAD 3031	Figure 2 GFP K1078Q	Δ*lacZ*::P_{chb}-GFP, Kan^R; igVCA0265/0266::CBS-mCherry v2, Cm^R; ΔchiS/cbp::$Carb^R$; ΔVCA0692::ChiS K1078Q, Tm^R
SAD 3032	Figure 2 GFP R1081Q	Δ*lacZ*::P_{chb}-GFP, Kan^R; igVCA0265/0266::CBS-mCherry v2, Cm^R; ΔchiS/cbp::$Carb^R$; ΔVCA0692::ChiS R1081Q, Tm^R
SAD 3033	Figure 2 GFP K1087Q	Δ*lacZ*::P_{chb}-GFP, Kan^R; igVCA0265/0266::CBS-mCherry v2, Cm^R; ΔchiS/cbp::$Carb^R$; ΔVCA0692::ChiS K1087Q, Tm^R
SAD 3034	Figure 2 GFP R1090Q	Δ*lacZ*::P_{chb}-GFP, Kan^R; igVCA0265/0266::CBS-mCherry v2, Cm^R; ΔchiS/cbp::$Carb^R$; ΔVCA0692::ChiS R1090Q, Tm^R
SAD 3035	Figure 2 GFP R1092Q	Δ*lacZ*::P_{chb}-GFP, Kan^R; igVCA0265/0266::CBS-mCherry v2, Cm^R; ΔchiS/cbp::$Carb^R$; ΔVCA0692::ChiS R1092Q, Tm^R
SAD 3036	Figure 2 GFP K1106Q	Δ*lacZ*::P_{chb}-GFP, Kan^R; igVCA0265/0266::CBS-mCherry v2, Cm^R; ΔchiS/cbp::$Carb^R$; ΔVCA0692::ChiS K1106Q, Tm^R
SAD 3037	Figure 2 GFP R1112Q	Δ*lacZ*::P_{chb}-GFP, Kan^R; igVCA0265/0266::CBS-mCherry v2, Cm^R; ΔchiS/cbp::$Carb^R$; ΔVCA0692::ChiS R1112Q, Tm^R
SAD 3038	Figure 2 GFP R1119Q	Δ*lacZ*::P_{chb}-GFP, Kan^R; igVCA0265/0266::CBS-mCherry v2, Cm^R; ΔchiS/cbp::$Carb^R$; ΔVCA0692::ChiS R1119Q, Tm^R
SAD 3039	Figure 2 GFP K1121Q	Δ*lacZ*::P_{chb}-GFP, Kan^R; igVCA0265/0266::CBS-mCherry v2, Cm^R; ΔchiS/cbp::$Carb^R$; ΔVCA0692::ChiS K1121Q, Tm^R
SAD 3040	Figure 2 GFP K1124Q	Δ*lacZ*::P_{chb}-GFP, Kan^R; igVCA0265/0266::CBS-mCherry v2, Cm^R; ΔchiS/cbp::$Carb^R$; ΔVCA0692::ChiS K1124Q, Tm^R
SAD 2675	Figure S2 $ChiS^{WT}$ No FLAG tag	Δ*lacZ*:P_{chb}-GFP, Kan^R; Δ*chiS/cbp*::$Carb^R$; ΔVCA0692::ChiS, Tm^R

Table S4. *Primers used in this study.*

Primer Name	Primer Sequence	Description
CKP 090	cggatccGGCTGCTAACAAAG	pHisTev amplify for FastClone F
BBC 2359	atggccctgaaaatacaggttttctatATGGCTGCCGCGCGGCACC	pHisTev amplify for FastClone R
CKP 713	CATatagaaaacctgtattttcagggccatTCGAAACAAGATTTGATGCG	ChiS DBD amplify for FastClone F
CKP 484	CCTTTCGGGCTTTGTTAGCAGCCggatccgTTATTCACTGGTCAGGAGTTTTTGC	ChiS DBD amplify for FastClone R
ABD 767	TTAATTTGGATCCCTGCGACACTC	ΔchiS F1 for Up arm
ABD 768	gtcgacggatccccggaatCAAAAAACGTGAGGAGAATGCC	ΔchiS R1 for Up arm
ABD 123	ATTCCGGGGATCCGTCGAC	$Carb^R$ cassette amplify F
ABD 124	TGTAGGCTGGAGCTGCTTC	$Carb^R$ cassette amplify R
ABD 798	gaagcagctccagcctacaGTACTGGATCTGAAACCAGTTAAG	Δcbp F2 for Down arm
ABD 799	GTATTGCGGAATGACCAGCATG	Δcbp R2 for Down arm
ABD 725	GAAGCAGCTCCAGCCTACA	Detect F for ΔchiS/cbp deletion
BBC 082	gtcgacggatccccggaatCATAACTTACACCTTACTCACCCAG	Detect R for ΔchiS/cbp deletion
BBC 832	GCTTTTTGCTACAACGACCG	ΔVCA0692 Tm^R F1 for Up arm
BBC 647	tttttctatttctgaatcgattcatacgaCTCATTAGGCACCCCAGGC	ΔVCA0692 Tm^R R1 for Up arm
BBC 1889	tcgtatgaatcgattcagaaatagaaaaaTTTGCCGCTTTTAACGTAAATCAG	ChiS F for Middle arm
BBC 577	tgtaggctggagctgcttcTTATTCACTGGTCAGGAGTTTTTGC	ChiS R for Middle arm
BBC 830	gaagcagctccagcctacaGTTGAGTTGGATGCAGCACC	ΔVCA0692 Tm^R F2 for Down arm
BBC 834	CACAATTTCTCGCTTAAAATGTCC	ΔVCA0692 Tm^R R2 for Down arm
DOG 0718	gcaggtggagcaggtggaCAACCGGTCTGGGTTTCTG	ChiS internal FLAG at E566 F
DOG 0717	tccaccacttccacctgcTTCTGAGACTTGATTAATAATGCGCAG	ChiS internal FLAG at E566 R
BBC 2274	gcaggtggaagtggtggagattataaggatgacgatgacaaagcaggtggagcaggtgga	1x FLAG Middle F
BBC 2275	tccacctgctccacctgctttgtcatcgtcatccttataatctccacc acttccacctgc	1x FLAG Middle R
ABD 332	GGCTGAACGTGGTTGTCGAAAATGAC	ΔlacZ F1 for Up arm
BBC 219	GTTTATTTTTGTCGACTGTACAGCGTTTAAATAGAGGTCGATATTGACCC	ΔlacZ R1 for Up arm
BBC 218	CGCTGTACAGTCGACAAAAATAAAC	Kan^R F Middle for GFP reporter
BBC 262	TACCGAGGACGCGAAGCTG	Kan^R R Middle for GFP reporter
BBC 266	CAGCTTCGCGTCCTCGGTAGAATAAAGCAATCCGCAAGCG	P_{chb} F Middle for GFP reporter
BBC 267	CCCGGGATCCTGTGTGAAATTGAGTTGCTTTCATTTCACTAATGG	P_{chb} R Middle for GFP reporter

BBC 252	CAATTTCACACAGGATCCCGGGAGGAGGTAACGTAATGCG TAAAGGAGAAGAAC	GFP F Middle for GFP reporter
BBC 254	tgtaggctggagctgcttcTTAGTTGTATAGTTCATCCATGCC	GFP R Middle for GFP reporter
ABD 255	gaagcagctccagcctacaCCACAATAAGCCAGAGAGCCTTAAG	ΔlacZ F2 for Down arm
ABD 256	CCCAAATACGGCAACTTGGCG	ΔlacZ R2 for Down arm
CKP 876	CCTCGGGCGAGTATCAATCGcagCAAGATTTGATGCGTGCC GTG	ChiS K1025Q F
CKP 877	CACGGCACGCATCAAATCTTGctgCGATTGATACTCGCCCGA GG	ChiS K1025Q R
CKP 878	CGGGCGAGTATCAATCGcag	ChiS K1025Q detect F
CKP 879	CAATCGAAACAAGATTTGATGCagGCCGTGTTAGTCGAAGC CATG	ChiS R1030Q F
CKP 880	CATGGCTTCGACTAACACGGCctGCATCAAATCTTGTTTCGA TTG	ChiS R1030Q R
CKP 881	CGAAACAAGATTTGATGCag	ChiS R1030Q detect F
CKP 882	GTGCCTTGAACTATTGGGAACagGTCTCAGGGCAAAGCAAG TTC	ChiS R1046Q F
CKP 883	GAACTTGCTTTGCCCTGAGACctGTTCCCAATAGTTCAAGGC AC	ChiS R1046Q R
CKP 884	CCTTGAACTATTGGGAACag	ChiS R1046Q detect F
CKP 885	GAACGAGTCTCAGGGCAAAGCcAgTTCACGTTTGCCGAACA AAG	ChiS K1052Q F
CKP 886	CTTTGTTCGGCAAACGTGAAcTgGCTTTGCCCTGAGACTCG TTC	ChiS K1052Q R
CKP 887	GAGTCTCAGGGCAAAGCcAg	ChiS K1052Q detect F
CKP 888	CGAACAAAGTGGCTTGTGGCagGTTTATCTTGACCGCAGCA C	ChiS R1063Q F
CKP 889	GTGCTGCGGTCAAGATAAACctGCCACAAGCCACTTTGTTC G	ChiS R1063Q R
CKP 890	AACAAAGTGGCTTGTGGCag	ChiS R1063Q detect F
CKP 891	GTGGCGCGTTTATCTTGACCagAGCACCCTACAAACTCGTA C	ChiS R1068Q F
CKP 892	GTACGAGTTTGTAGGGTGCTctGGTCAAGATAAACGCGCCA C	ChiS R1068Q R
CKP 893	GGCGCGTTTATCTTGACCag	ChiS R1068Q detect F
CKP 894	CCGCAGCACCCTACAAACTCagACCCTAGACAAATACTTAC GAATTG	ChiS R1074Q F
CKP 895	CAATTCGTAAGTATTTGTCTAGGGTctGAGTTTGTAGGGTGC TGCGG	ChiS R1074Q R
CKP 896	GCAGCACCCTACAAACTCag	ChiS R1074Q detect F
CKP 897	CTACAAACTCGTACCCTAGACcAgTACTTACGAATTGAGACA CTG	ChiS K1078Q F
CKP 898	CAGTGTCTCAATTCGTAAGTAcTgGTCTAGGGTACGAGTTTG TAG	ChiS K1078Q R

CKP 899	CAAACTCGTACCCTAGACcAg	ChiS K1078Q detect F
CKP 900	CTCGTACCCTAGACAAATACTTACagATTGAGACACTGCCTAAAAC	ChiS R1081Q F
CKP 901	GTTTTAGGCAGTGTCTCAATctGTAAGTATTTGTCTAGGGTACGAG	ChiS R1081Q R
CKP 902	CGTACCCTAGACAAATACTTACag	ChiS R1081Q detect F
CKP 903	CTTACGAATTGAGACACTGCCTcAgACACCGCGTTGGCGAAC	ChiS K1087Q F
CKP 904	GTTCGCCAACGCGGTGTcTgAGGCAGTGTCTCAATTCGTAAG	ChiS K1087Q R
CKP 905	GAATTGAGACACTGCCTcAg	ChiS K1087Q detect F
CKP 906	GACACTGCCTAAAACACCGCagTGGCGAACCGTACTGAACTC	ChiS R1090Q F
CKP 907	GAGTTCAGTACGGTTCGCCActGCGGTGTTTTAGGCAGTGTC	ChiS R1090Q R
CKP 908	CACTGCCTAAAACACCGCag	ChiS R1090Q detect F
CKP 909	CCTAAAACACCGCGTTGGCagACCGTACTGAACTCGCTCGAC	ChiS R1092Q F
CKP 910	GTCGAGCGAGTTCAGTACGGTctGCCAACGCGGTGTTTTAGG	ChiS R1092Q R
CKP 911	CTAAAACACCGCGTTGGCag	ChiS R1092Q detect F
CKP 912	CGACTACATTCTTGAGCATTGCcAgGAAGCAGGCCCTGAACGC	ChiS K1106Q F
CKP 913	GCGTTCAGGGCCTGCTTCcTgGCAATGCTCAAGAATGTAGTCG	ChiS K1106Q R
CKP 914	TACATTCTTGAGCATTGCcAg	ChiS K1106Q detect F
CKP 915	CAAAGAAGCAGGCCCTGAACagACTCACATCGAAATGCAGCG	ChiS R1112Q F
CKP 916	CGCTGCATTTCGATGTGAGTctGTTCAGGGCCTGCTTCTTTG	ChiS R1112Q R
CKP 917	AAGAAGCAGGCCCTGAACag	ChiS R1112Q detect F
CKP 918	CACTCACATCGAAATGCAGCagGATAAATTGCAAAAACTCCTGACC	ChiS R1119Q F
CKP 919	GGTCAGGAGTTTTTGCAATTTATCctGCTGCATTTCGATGTGAGTG	ChiS R1119Q R
CKP 920	CTCACATCGAAATGCAGCag	ChiS R1119Q detect F
CKP 921	CACATCGAAATGCAGCGCGATcAgTTGCAAAAACTCCTGACCAGTG	ChiS K1121Q F
CKP 922	CACTGGTCAGGAGTTTTTGCAAcTgATCGCGCTGCATTTCGATGTG	ChiS K1121Q R
CKP 923	TCGAAATGCAGCGCGATcAg	ChiS K1121Q detect F
CKP 924	GAAATGCAGCGCGATAAATTGCAAcAgCTCCTGACCAGTG	ChiS K1124Q F
CKP 925	CACTGGTCAGGAGcTgTTGCAATTTATCGCGCTGCATTTC	ChiS K1124Q R
CKP 926	AGCGCGATAAATTGCAAcAg	ChiS K1124Q detect F
CKP 642	GGTATTTTGACGTTAATGACGTAGGGCATCTAGGTTTTGACGTTTTTAACGGGAATTGCA	P_{chb} WT 60 bp EMSA probe F

CKP 643	TGCAATTCCCGTTAAAAACGTCAAAACCTAGATGCCCTACG TCATTAACGTCAAAATACC	P_{chb} WT 60 bp EMSA probe R
CKP 648	GGTATTTTGAtacTAATGACGTAGGGCATCTAGGTTTTGAtacT TTTAACGGGAATTGCA	P_{chb} Mutated 60 bp EMSA probe F
CKP 649	TGCAATTCCCGTTAAAAgtaTCAAAACCTAGATGCCCTACGT CATTAgtaTCAAAATACC	P_{chb} Mutated 60 bp EMSA probe R
CKP 978	AAAATCAGGCTAGTGAGCGAG	P_{chb} Bend probe 1 F
CKP 979	TATCAATTGCAATTCCCGTTAAAAACG	P_{chb} Bend probe 1 R
CKP 980	ATATAACTCAGGCAAAGAGCC	P_{chb} Bend probe 2 F
CKP 981	AGGAGTAAGAAAACACCTAGCC	P_{chb} Bend probe 2 R
CKP 982	CAAGGCCAAATAAGTAAGTAAAC	P_{chb} Bend probe 3 F
CKP 983	GGAGTCATGAGTGGCCTGTAG	P_{chb} Bend probe 3 R
CKP 984	AACCTAGCTAAACCGTACCC	P_{chb} Bend probe 4 F
CKP 985	CCTCATCACTTTTACCCCGTC	P_{chb} Bend probe 4 R
CKP 986	TTGAATCACTTCGCGTTTTTTG	P_{chb} Bend probe 5 F
CKP 987	CATCAATTGATAAACACTCTCCAAG	P_{chb} Bend probe 5 R
CKP 988	TCACACATCAGAAGGTATTTTG	P_{chb} Bend probe 6 F
CKP 989	TTGCTTTCATTTCACTAATGGATGG	P_{chb} Bend probe 6 R
CKP 990	GACGTAGGGCATCTAGGTTTTG	P_{chb} Bend probe 7 F
CKP 991	ATATTGGCAAGCATAGCTGTTCC	P_{chb} Bend probe 7 R
BBC 989	GCATCTAGGTTTTGACGTTTTTAACG	P_{chb} amplify for ChIP qPCR F
BBC 990	AACACTCTCCAAGACCTACCTC	P_{chb} amplify for ChIP qPCR R
ABD 132	CTGTCTCAAGCCGGTTACAA	*rpoB* amplify for ChIP qPCR F
ABD 133	TTTCTACCAGTGCAGAGATGC	*rpoB* amplify for ChIP qPCR R